





## Motion envelopes: unfolding longitudinal rotation data from walking stick-figures

Ivo F. Roupa<sup>a</sup>, Sérgio B. Gonçalves<sup>a</sup>, Miguel Tavares da Silva<sup>a</sup> , Richard R. Neptune<sup>b</sup> and Daniel Simões Lopes<sup>c</sup> 

<sup>a</sup>IDMEC, Instituto Superior Técnico, Universidade de Lisboa, Lisbon, Portugal; <sup>b</sup>Walker Department of Mechanical Engineering, The University of Texas at Austin, Austin TX, USA; <sup>c</sup>INESC ID, Instituto Superior Técnico, Universidade de Lisboa, Lisbon, Portugal

### ABSTRACT

This work presents Motion Envelopes (ME), a simple method to estimate the missing longitudinal rotations of minimal stick figures, which is based on the spatial-temporal surface traced by line segments that connect contiguous pairs of joints. We validate ME by analyzing the gait patterns of 6 healthy subjects, comprising a total of 18 gait cycles. A strong correlation between experimental and estimated data was obtained for lower limbs and upper arms, indicating that ME can predict their longitudinal orientation in normal gait, hence, ME can be used to complement the kinematic information of stick figures whenever it is incomplete.

### ARTICLE HISTORY

Received 15 June 2021  
Accepted 7 December 2021

### KEYWORDS

Inverse kinematics; stick figures; longitudinal rotations; markerless systems; gait

## Introduction

Kinematic analysis plays an important role in the quantitative evaluation of human movement in several fields of research, such as non-pathological and pathological analysis of human motion (Ludewig and Cook 2000; Quental et al. 2018), gait (Sutherland 2002), sports (Bezodis et al. 2020; Genevois et al. 2020), rehabilitation (Safaeepour et al. 2014; Taylor et al. 2020), or ergonomics (McDonald et al. 2019; Harari et al. 2020) settings. To perform a proper kinematic analysis, it is necessary to track the motion to obtain the spatial-temporal information of the human movement.

High end commercial marker-based motion capture systems track the three dimensional (3D) nature of human motion. In contrast, markerless systems only provide an estimation of the position of the human joint centres and some ending points (e.g., tip of the head, hands and toes), which are then used to build stick figures with a minimal set of points (Shotton et al. 2013; Cao et al. 2017; Mehta et al. 2017, 2020), i.e., body segments are represented by a line connecting two points, either joint centres or other ending points, thus resulting in an abstract representation of the human body usually referred to as a ‘stick figure’ (Shotton et al. 2013; Cao et al. 2017; Mehta et al. 2017, 2020).

The advantages of markerless systems are that they require simple acquisition protocols and the kinematic information can be easily obtained in real-time, making them the ideal solution for clinical and rehabilitation applications (Kobsar et al. 2019; Lopes et al. 2019; Alves et al. 2020; Chakraborty et al. 2020; Worthen-Chaudhari et al. 2020). Despite these advantages, markerless systems tend to present accuracy problems due to errors during the determination of the spatial location of the joints and to segments occlusions, leading to badly estimated 3D orientations of body segments (Cai et al. 2019; Çubukçu et al. 2020).

Although commonly used in the analysis of human movement, minimal stick figure representations do not provide the needed kinematic information to compute the six degrees-of-freedom (DoF) of each segment in space. Since each ‘stick’ is defined only by two points and considering that at least three non-collinear points are required to fully define the orientation of the local reference frame of a body segment in space, the kinematic analysis of stick figure models inherently results in an ill-posed problem. Nevertheless, several studies have investigated the accuracy and reliability of kinematic analysis in normal (Geerse et al. 2015) and pathological (Ma et al. 2019) gait, or to evaluate the drop jump (Guess et al. 2017) using stick figures. In such studies, the accuracy

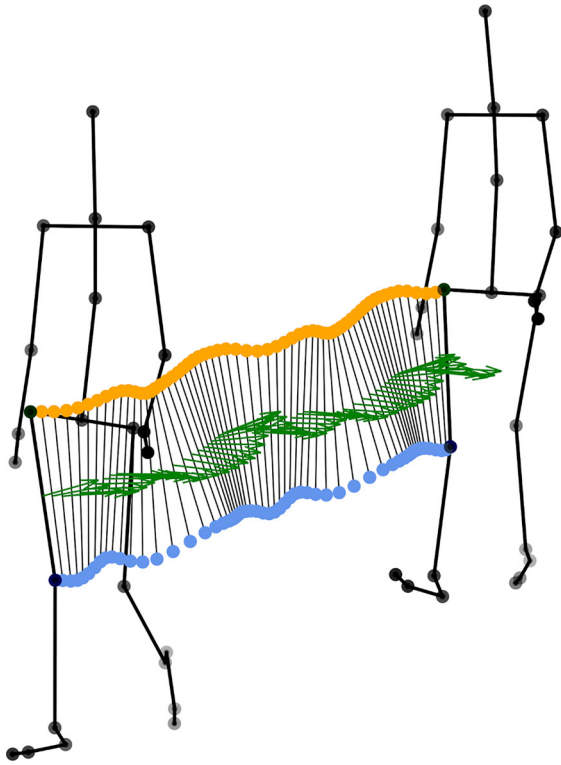


**Figure 1.** Motion Envelope of the right thigh in two consecutive strides: stick-figure of the first (black) and last (black) frames with the joints of interest represented in orange and blue (spheres). The motion of the thigh is represented by (black) segments connecting the knee and hip markers in each time frame and the corresponding normal vectors (green).

of spatial-temporal and kinematic variables vary from modest to excellent between the data obtained using the stick figure and a full-body model for spatial-temporal parameters and for some kinematic variables, particularly in sagittal and frontal planes (Geerse et al. 2015; Guess et al. 2017; Cai et al. 2019; Ma et al. 2019). However, poor correlations were found for the longitudinal rotations of upper and lower body segments (Cai et al. 2019; Matias et al. 2021).

In this work, the use of the Motion Envelopes (ME) geometric method is explored to overcome the lack of kinematic information that resides in minimal stick figure representations. (e.g., stick figures with limb segments represented by only 2 points). The seminal concept underlying Motion Envelopes is that, due to spatial and temporal coherence, the axial rotation of any segment may be estimated by computing the normal vector to the surface generated by a line segment through space and time (Zhang et al. 2018; Gammon and Menon 2020). Such geometric information would allow for the definition of a local reference frame for each segment (Schneider and Eberly 2003; Lopes et al. 2013), thus solving the minimal

representation of the human body model and presenting an alternative to marker-based systems. Hence, the main objective of this study is the validation of the ME geometric method for analyzing normal human gait. For that purpose, the estimated ME longitudinal rotations will be compared with real rotation data from a full-body model acquired from a marker-based system that is considered our gold standard. To discard possible experimental errors, the orientations computed using the two methods will consider the same data pool. However, only the coordinates of the joints and other relevant points of the biomechanical model will be used in the ME model. Therefore, the differences observed in the data will express deviations intrinsic to the method and not due to experimental errors associated with different acquisition systems.

## Methods

### Motion envelopes

ME is a geometric method that generates a surface based on the line segment defined by two points that compose a body segment, obtained by linear interpolation of the trajectories traced through time. Thus, this surface is defined by tracing the longitudinal line ( $\mathbf{v}_L$ ) that represents the segment throughout time (see Figure 1). By computing the normal vector to this surface ( $\mathbf{v}_{ME}^\perp$ ), it is then possible to determine a third vector perpendicular by applying a cross-product between the previous ones and, therefore, to estimate the 3D orientation of the local reference frame of the segment, thus, it is possible to estimate a 3D global reference frame per segment that evolves in space and time. This geometric tool comprises the computation of a vector that is non-collinear ( $\mathbf{v}_{ME}^*$ ) to the vector that define the segment in analysis ( $\mathbf{v}_L$ ). Figure 2 presents the Motion Envelope (black surface) of the right thigh and its respective normal vector (green vector).

The first step of the method is to generate ME surfaces based on the motions of the corresponding body (line) segments in space. Each ME surface is obtained by tracing a line segment between points  $P_1$  and  $P_2$  (i.e., proximal and distal segment joints) that define the longitudinal direction of the body segment throughout time, as schematically represented in Figure 2. Accordingly, the longitudinal vector ( $\mathbf{v}_L$ ) can be calculated as:

$$\mathbf{v}_L = \mathbf{r}_2 - \mathbf{r}_1 \quad (1)$$

where  $\mathbf{r}_1$  and  $\mathbf{r}_2$  are the position vectors with the 3D Cartesian coordinates of points  $P_1$  and  $P_2$ .

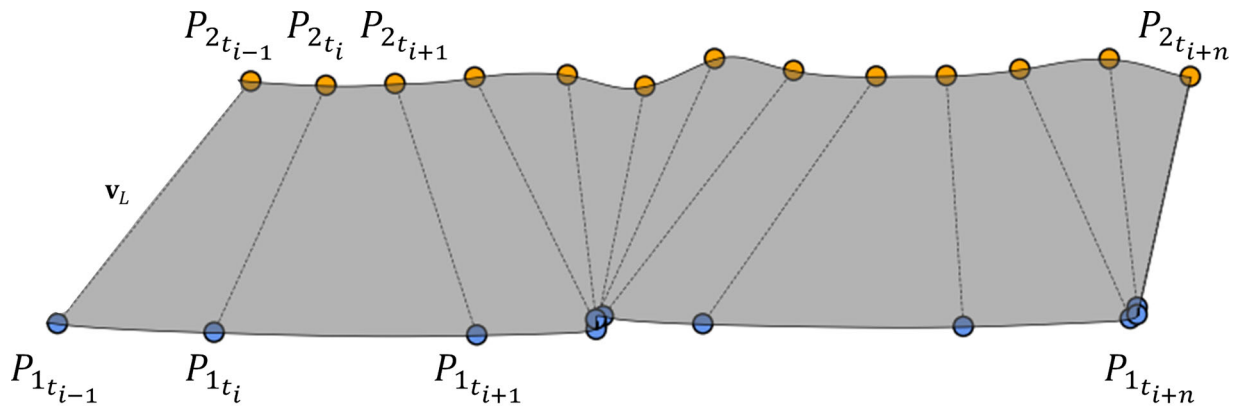


**Figure 2.** Representation of the Motion Envelope surface for the thigh segment (in grey), defined using the 3D Cartesian coordinates of points  $P_1$ , located at the knee (blue circles), and  $P_2$ , located at the hip (orange circles), and connected by longitudinal vector  $\mathbf{v}_L$  (dashed).

The second step uses the definition of two auxiliary planes of motion,  $ME_1$  and  $ME_2$ , for each time frame  $t_i$ , as depicted in Figure 3. The first plane ( $ME_1$ ) is defined using vector  $\mathbf{v}_L$  at time frame  $t_i$  and the displacement vector of point  $P_1$  from the previous time frame  $t_{i-1}$  to the current time frame  $t_i$ . The second plane ( $ME_2$ ) is defined in a similar way, however, the displacement vector of point  $P_2$ , calculated from the current time frame  $t_i$  to the next time frame  $t_{i+1}$ , is used instead.

Hence, for instant  $t_i$ , the vectors normal to each plane are computed, using the cross product:

$$\mathbf{v}_{ME_1}^\perp = \mathbf{v}_L \times (\mathbf{r}_{1t_i} - \mathbf{r}_{1t_{i-1}}) \quad (2)$$

$$\mathbf{v}_{ME_2}^\perp = \mathbf{v}_L \times (\mathbf{r}_{2t_{i+1}} - \mathbf{r}_{2t_i}) \quad (3)$$

For the same instant  $t_i$ , the orientation of the vector normal to the surface ( $\mathbf{v}_{ME}^\perp$ ), is then obtained by calculating the average between the two normal vectors:

$$\mathbf{v}_{ME}^\perp = \frac{1}{2} (\mathbf{v}_{ME_1}^\perp + \mathbf{v}_{ME_2}^\perp) \quad (4)$$

Finally, the three orthogonal unit vectors that define the local reference frame of each segment can be computed:

$$\mathbf{v}_z = \frac{\mathbf{v}_L}{|\mathbf{v}_L|} \quad (5)$$

$$\mathbf{v}_y = \frac{\mathbf{v}_{ME}^\perp}{|\mathbf{v}_{ME}^\perp|} \quad (6)$$

$$\mathbf{v}_x = \mathbf{v}_y \times \mathbf{v}_z \quad (7)$$

Finally, these vector calculations (Equations 1-7) are applied to each body segment, which render several MEs for a single stick figure.

### Experimental data acquisition

The applicability of the ME method in the estimation of the segments' orientations was evaluated by applying it to the gait patterns of six healthy volunteers (age:  $25.4 \pm 7.74$ , height:  $1.70 \pm 0.10$ , weight:  $62.6 \pm 11.1$ ) for a total of 18 gait cycles. The experimental procedures used in this study were previously approved by the IST Ethics Committee (Ref. 1/2020 CE-IST). All subjects gave their written informed consent after a detailed explanation of the experimental protocol and before the beginning of the study.

Kinematic data was acquired in the Lisbon Biomechanics Laboratory at Instituto Superior Técnico using an optoelectronic motion capture system composed by 14 Infrared ProReflex 1000 cameras (Qualisys©, Göteborg, Sweden), set to an acquisition frequency of 100 Hz. Prior to the data acquisition, all subjects had an adaptation period to the experimental setup. Afterwards, a 15-second static trial was performed followed by three valid gait cycles for each leg.

### Biomechanical models

A 3D full-body biomechanical model with 16 anatomical segments (see Figure 4a) was implemented to serve as ground-truth for comparing the results obtained from the ME method to the stick-figure model (see Figure 4b) created to represent the type of kinematic data commonly obtained by markerless single camera systems (Shotton et al. 2013). A marker set protocol with 68 retro-reflective spherical markers, including calibration and tracking markers, was utilized to acquire the movements of the six subjects (see Figure 4c). The elbow, wrist, knee, and ankle

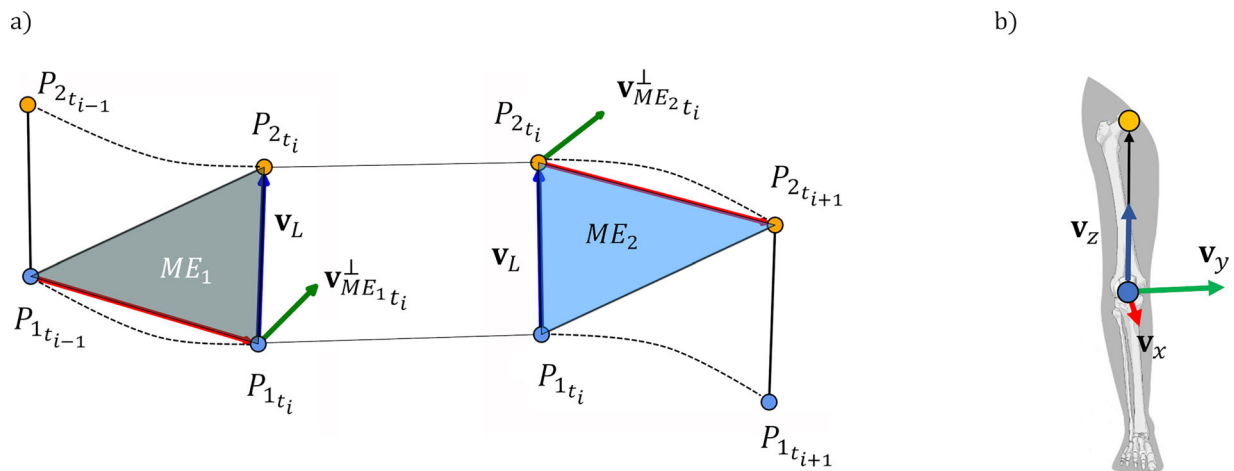


**Figure 3.** Triangulation steps for the thigh segment: a) calculation of the vectors normal to plane  $ME_1$  and  $ME_2$  considering the time frames  $t_{i-1}$ ,  $t_i$  and  $t_{i+1}$ ; b) definition of the body segment orientation.

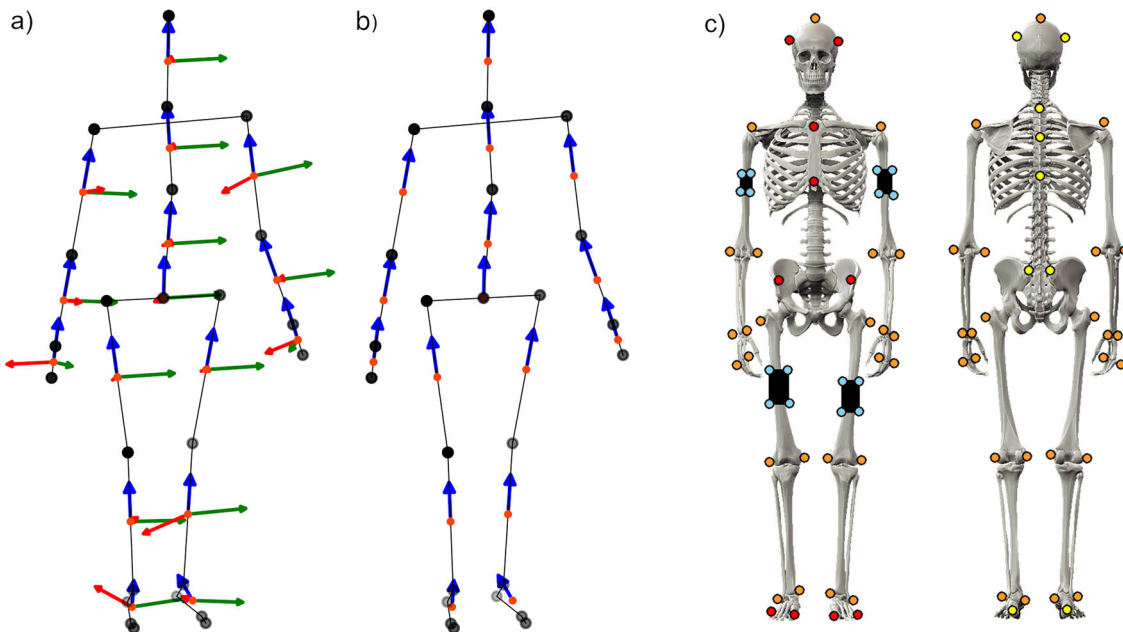


**Figure 4.** (a) full-body biomechanical model – black dots depict the points used to define the model and the red, green and blue vectors represent the anterior-posterior, medial-lateral and longitudinal vectors of each segment, respectively; (b) stick figure model – black points and lines depict the “stick figure” representing the human body, while blue vectors represent the segments longitudinal vectors; (c) marker set protocol – red and yellow points represent reflective markers seen from an anterior or from a posterior view, respectively, orange points represent markers seen in both views and blue points are tracking markers placed on rigid plates.

joint centers were computed as the midpoint of the retro reflective markers placed on lateral and medial bony landmarks (see Figure 4c), while the hip joint center was computed using the regression method proposed by Davis et al. (Davis et al. 1991). Furthermore, the trajectories of the elbow and knee markers were reconstructed using clusters of markers placed on the thigh and upper arm. The definition of

the local reference frames of each segment followed the recommendations provided by the International Society of Biomechanics (ISB) (Wu et al. 2002, 2005).

Figure 4 (a) full-body biomechanical model – black dots depict the points used to define the model and the red, green and blue vectors represent respectively the anterior-posterior, medial-lateral and longitudinal vectors of each segment; (b) stick figure model – black

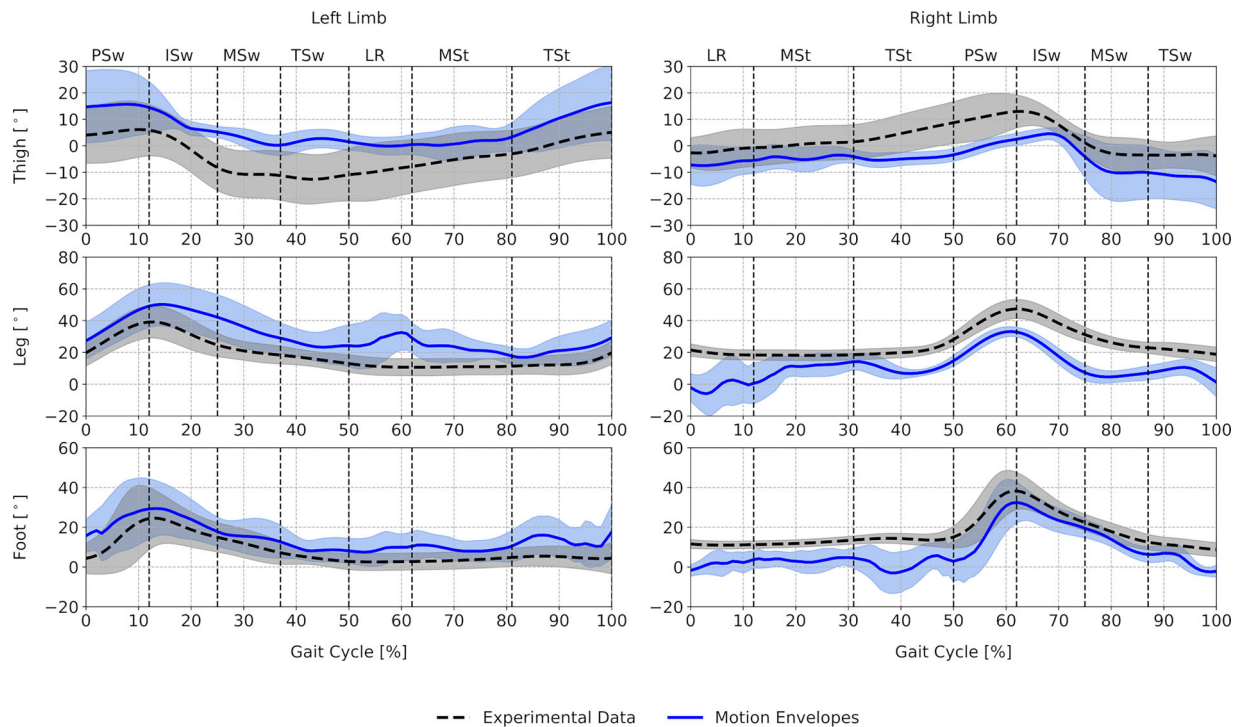


**Figure 5.** Representation of the angle between the medial-lateral vector and the global reference frame for the full-body (blue) and stick figure model (black) along the gait cycle for a right stride (shaded region indicates  $\pm 1$  standard deviation of the experimental data).

**Table 1.** MAE and maximum absolute error between the medial-lateral vectors computed using the two methods along the gait cycle.

Angular Position (°)	Thigh		Leg		Foot		Upper Arm		Fore Arm		Hand	
	R	L	R	L	R	L	R	L	R	L	R	L
Max (raw)	12.1	15.3	26.0	21.8	17.4	13.2	17.7	20.8	56.9	58.7	66.6	65.7
Max (corrected)	4.8	5.5	11.5	10.3	8.9	7.0	4.8	4.9	23.2	25.2	25.4	25.2
Mean (raw)	7.3	9.9	14.5	11.5	8.6	6.2	13.0	16.0	36.0	34.0	46.0	41.0
Mean (corrected)	2.2	2.3	4.5	3.2	2.8	1.9	3.3	1.8	13.3	15.9	14.6	15.5

points and lines depict the “stick figure” representing the human body, while blue vectors represent the segments longitudinal vectors; (c) marker set protocol – red and yellow points represent reflective markers seen from an anterior or from a posterior view, respectively, orange points represent markers seen in both views and blue points are tracking markers placed on rigid plates.

### Data processing

The coordinates of the markers were filtered using a 2<sup>nd</sup> order low-pass Butterworth filter with a cut-off frequency of 6 Hz. Segment orientations were posteriorly calculated using the ISB recommendations, for the first model, and the proposed ME method for the later. Hence, for the later model solely the joint coordinates and distal points were used for the calculation of the segments’ orientations, i.e., no auxiliary markers were used in the calculation of the orientation of the model’s segments.

Segments’ orientations, computed using both methodologies, were compared by calculating the angle between the medial-lateral vectors ( $v_y$ ) of both models (see Figures 4a and 3b, respectively) and the medial-lateral direction of the global reference frame. With the results obtained for these angles, the mean absolute error (MAE) between the two data sets was calculated throughout the gait cycle. Additionally, the Pearson correlation coefficient (PCC) between the two medial-lateral angles throughout the gait cycle was also computed. All calculations were performed using custom scripts written in MATLAB (MathWorks©, Natick, MA) and Python 3.7 (van Rossum and Drake 2006).

### Results

The proposed ME method enabled the estimation of the segments orientation of a stick figure model during gait movements. However, the reliability of the results varied

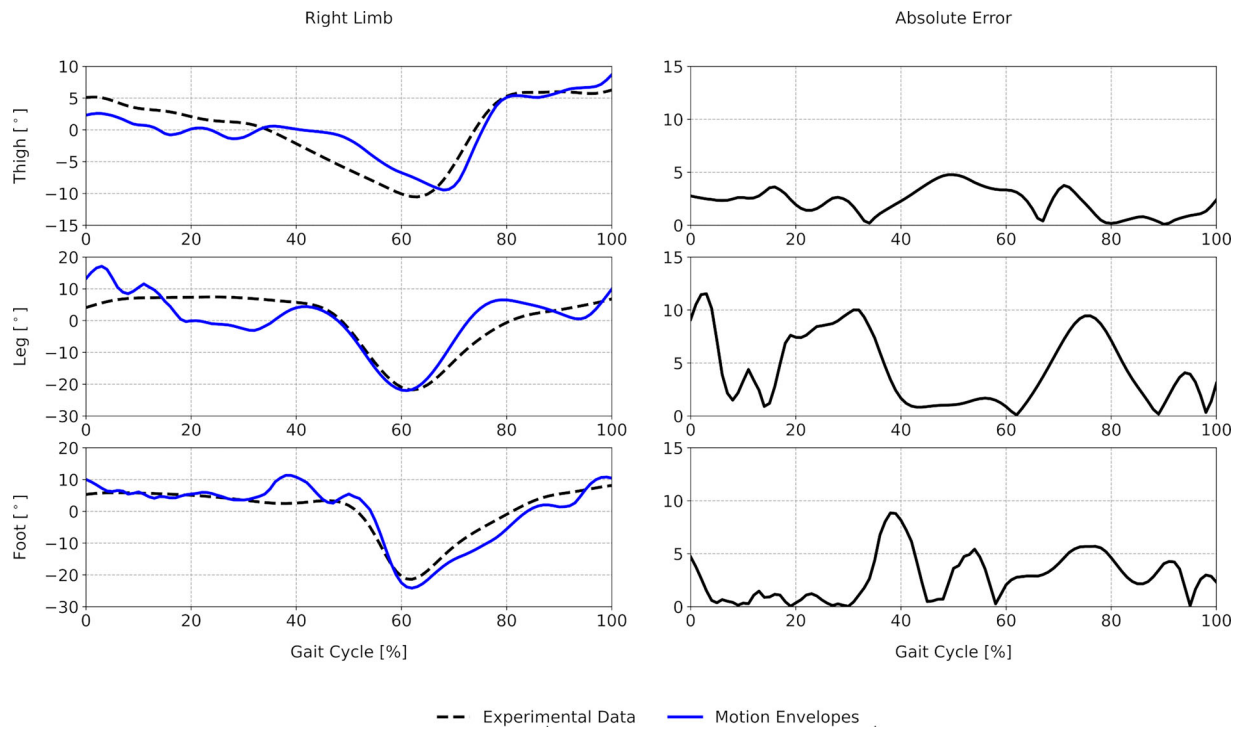


**Figure 6.** Representation of the segments orientation with the offset correction: Left) angle between the medial-lateral vector and the global reference frame for the full-body (blue) and stick figure model (black); Right) absolute error between orientations along the gait cycle.

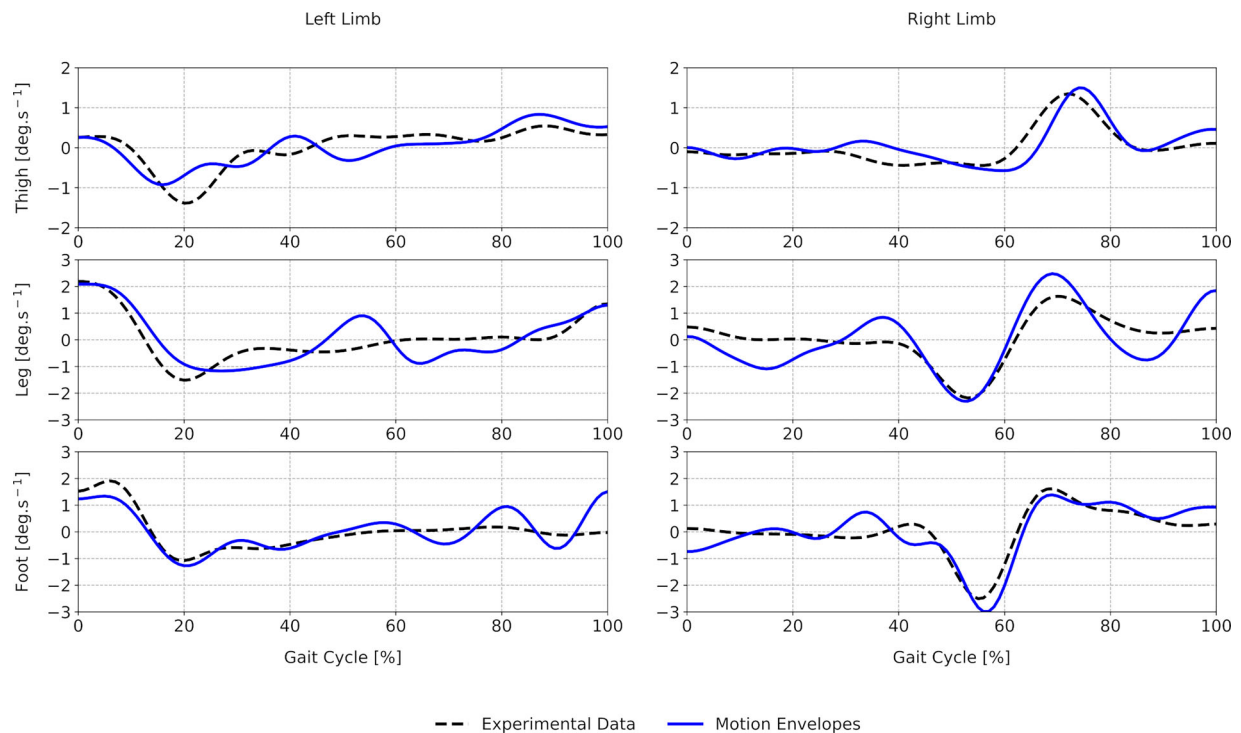


**Figure 7.** Representation of the first time derivative of the angle between the medial-lateral vector and the global reference frame for the full-body (blue) and stick figure model (black) along the gait cycle for a right stride.

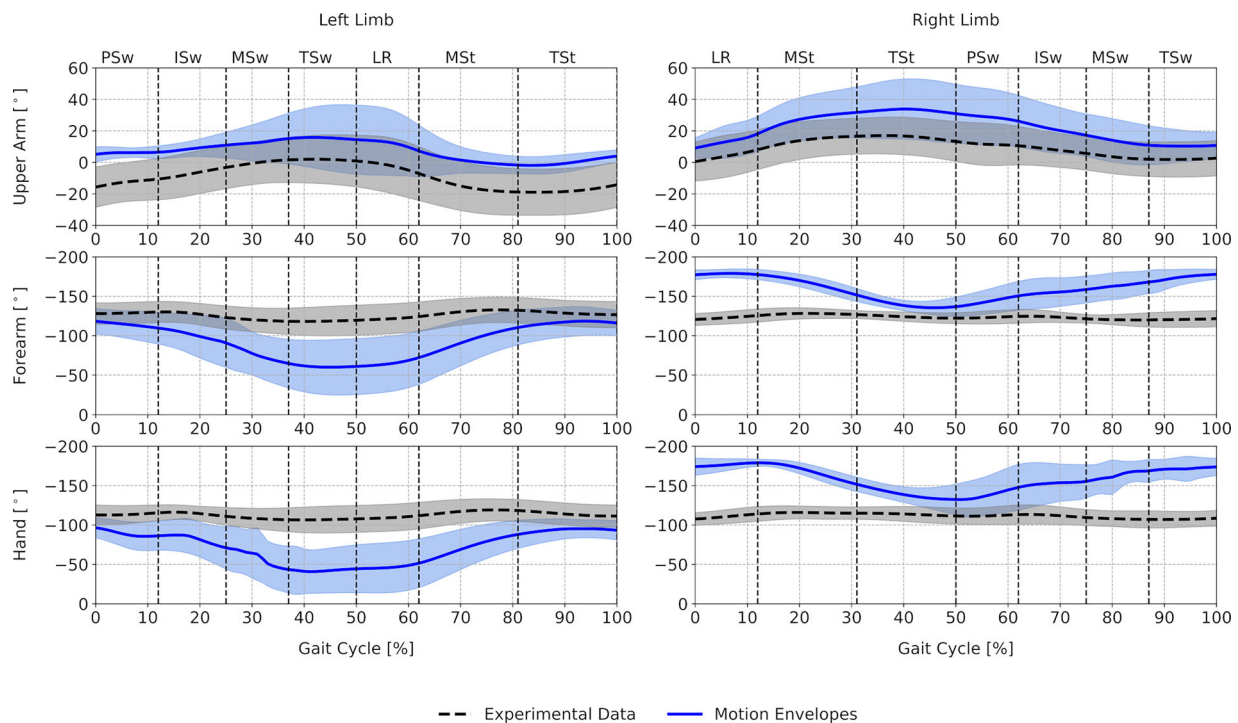


**Figure 8.** Representation of the angle between the medial-lateral vector and the global reference frame for the full-body (blue) and stick figure model (black) along the gait cycle for a right stride (shaded region indicates  $\pm 1$  standard deviation of the experimental data).

across segments. In general, the orientations for the lower limbs followed the patterns observed in the full-body model used as ground-truth. The same can no longer be stated for the results obtained for the upper limbs, in particular for the forearm and hand, in which a non-consistent patterns were obtained with respect to the full-body model.

### Lower limbs

The orientation of the medial-lateral vector for the lower limbs shows a smooth trajectory throughout the gait cycle (see Figure 5). This pattern was already expected, as the walking movement is not characterized by abrupt longitudinal rotations. A comparison of the segments' orientation computed using the two methods indicates the existence of similar patterns for all analyzed segments, which is supported by the strong to very strong positive correlation observed in the thigh (right:  $r=0.882$ ,  $p<.001$ ; left:  $r=0.904$ ,  $p<.001$ ), shank (right:  $r=0.813$ ,  $p<.001$ ; left:  $r=0.917$ ,  $p<.001$ ) and foot (right:  $r=0.939$ ,  $p<.001$ ; left:  $r=0.935$ ,  $p<.001$ ) segments. Regarding the MAE, the foot segment presented the lowest value ( $8.6^\circ$ ), followed by the thigh ( $9.9^\circ$ ) and finally by the leg ( $14.5^\circ$ ) (see Table 1).

Despite the existence of a strong correlation between the two methods, the results show a vertical

shift between curves, which varied with the segment in analysis. These differences can be explained by the inability of the ME method in estimating the initial orientation of the segment. Hence, to better compare the curves, their mean value was calculated and removed (see Figure 6). This procedure allowed for the decrease of the MAE to values around  $2.2^\circ$  for the thigh,  $4.5^\circ$  for the shank and  $2.8^\circ$  for the foot. Likewise, the maximum error along the cycle decreased to values near  $5.5^\circ$ ,  $11.5^\circ$  and  $8.9^\circ$  respectively to the thigh, shank, and foot segments (see Table 1).

The applicability of the ME method in gait is also supported by the analysis of the first time derivative of both curves (see Figure 7), which indicates the existence of a strong correlation between the two methods for all lower limb segments, thigh (right:  $r=0.832$ ,  $p<.001$ ; left:  $r=0.759$ ,  $p<.001$ ), shank (right:  $r=0.812$ ,  $p<.001$ ; left:  $r=0.818$ ,  $p<.001$ ) and foot (right:  $r=0.899$ ,  $p<.001$ ; left:  $r=0.809$ ,  $p<.001$ ) segments.

An analysis of the variability of the curves shows that the full body method tends to present a more uniform variability along the cycle, while the standard deviation in the ME method varied across the gait cycle. A higher variability is also found in the ME method, in particular for the leg and foot segments (see Figure 5).

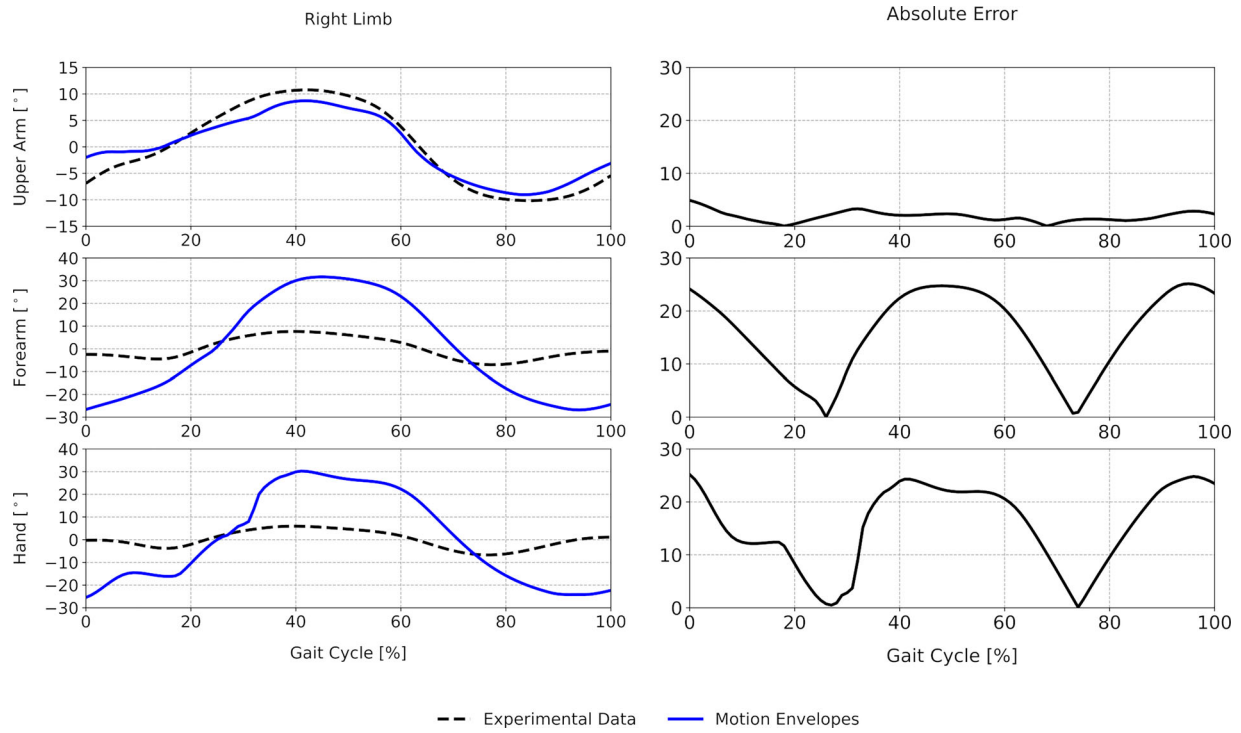


**Figure 9.** Representation of the segments orientation considering the offset correction: Left) angle between the medial-lateral vector and the global reference frame for the full-body (blue) and stick figure model (black); Right) absolute error between orientations along the gait cycle.

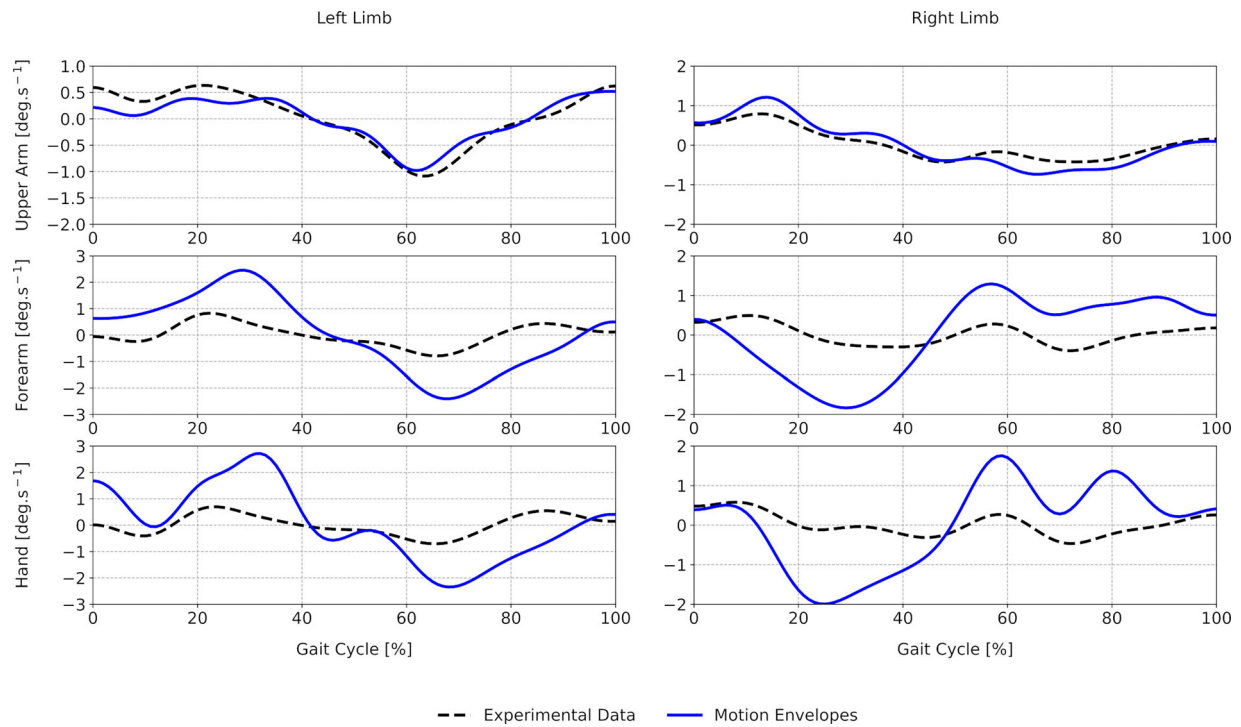


**Figure 10.** Representation of the first time derivative of the vector between the medial-lateral vector and the global reference frame for the full-body model (blue) and stick figure model (black) along the gait cycle for a right stride.



## Upper limbs

The upper arm orientation was characterized by a progressive external rotation movement from the terminal swing phase until the terminal stance phase, followed by an internal rotation movement in the subsequent phases (see Figure 8). The ME method was able to predict this behavior, resulting in a pattern similar to the one obtained using the full-body model (see Figure 8). These findings are supported by the very strong correlation observed between the two methods (right:  $r=.983$ ,  $p<.001$ ; left:  $r=.984$ ,  $p<.001$ ). A MAE of  $16^\circ$  was achieved for the upper arm that decreased to  $3.3^\circ$ , when the mean of the signals was removed (see Figure 9). The value for the maximum absolute error, considering the offset correction, was approximately  $5^\circ$  (see Table 1). The comparison of the first time derivative calculated for both methods also indicates the existence of a strong correlation for the upper arm (right:  $r=.965$ ,  $p<.001$ ; left:  $r=.952$ ,  $p<.001$ ), suggesting that the variation of the orientation along time estimated using the ME method is consistent with the full-body model (see Figure 10).

The ME was not able to depict the forearm longitudinal rotations along the cycle. The pattern obtained using the full-body model shows small variations in the orientation of the forearm, indicating that the forearm is rotating to counteract the upper arm longitudinal rotation described above. In contrast, the ME predicted a variation in the forearm orientation similar to the one observed in the upper arm, implying that no significant rotations occurred at the forearm segment to compensate the upper arm internal and external rotation (see Figure 8). These differences resulted in lower correlation values for this segment (right:  $r=.230$ ,  $p<.05$ ; left:  $r=.718$ ,  $p<.001$ ), as well as a MAE of  $15.9^\circ$  even when the mean signal was removed (see Figure 9 and Table 1). A similar trend was observed for the hand segment. Since no longitudinal movement occurred at the wrist joint, the orientation obtained for the hand using the ME method followed the orientation predicted to the forearm segment (see Figure 8 and Table 1). In this segment the following correlation was obtained, (right:  $r=.183$ ,  $p>.005$ ; left:  $r=.594$ ,  $p<.001$ ).

As for the lower limbs, the analysis of inter-variability for the upper limbs segments shows higher standard deviation values in the ME method and more variations along the gait cycle.

## Discussion

The present work explores the utility of the ME method in estimating the global orientation of limb

segments of minimal stick figures during gait cycle. ME unfolds the geometric relations from the spatial-temporal surface described by body segment movements, enabling the computation of a vector normal to the plane of movement defined by tracing the segment in space throughout time. The variations in the vector orientation represents the temporal evolution of the local reference frame of the segment during movement. By extracting these geometric relations from the movement patterns, it is possible to complement the kinematic data of minimal stick figures with the missing longitudinal rotations.

The ME method allowed for the successful estimation of the global orientations of the thigh and leg segments along the gait cycle, presenting a strong to very strong correlation with the full-body biomechanical model. Regarding the upper limb, results show only a strong correlation for the upper arm. ME did not predict the longitudinal rotation that occurred at the forearm segment to counteract the upper arm rotation. Despite the strong correlation observed in the lower limbs, the results show a noticeable offset in the segments orientation between the two methods. This difference can be explained by the incapacity of the ME method in estimating the initial angular position of the segment longitudinal rotation. This issue limits the application of ME to estimate the magnitude of the longitudinal rotations associated with the movement. However, it can be used to predict the variation of the longitudinal rotation along the cycle and to estimate its angular amplitude. This idea is supported by the strong correlation between the two methods. Furthermore, when the offset was removed, either by removing the average of the signal or by comparing its first derivative both patterns followed the same trend, in particular the upper arm and lower limbs.

Moreover, ME is computationally efficient since it relies on simple geometric relations between vectors, which make ME suitable for real-time applications. Additionally, ME can be applied to data coming from different sources, as it only requires the coordinates of the points that define the stick figure model. The versatility and computational efficiency of the ME method enables its use in tandem with acquisition systems based on inexpensive and portable cameras, complementing the kinematic information provided by them. This feature is of utmost interest for clinical and rehabilitation applications, since besides the limitations previously noted for the high-end motion capture systems, they require additional equipment that can interfere with the movement under analysis.

Despite its advantages, ME presents some limitations that do not allow its use to substitute the usual methods for computing the 3D orientation of the body segments in biomechanical models defined with three non collinear points. ME cannot predict the initial angular position of the segment and, consequently, cannot determine the value of the angular displacement associated to the movement. Moreover, ME presents a poor accuracy when applied in the study of movements with pure axial rotations (as seen in the lower correlations observed in the forearm segments), as from a geometric point-of-view, a pure longitudinal rotation does not imply a variation in the orientation of the ME surface. Hence, the normal vector that is computed posteriorly will not depict the movement that is occurring.

The ME can also present problems for static or very slow movements, as the displacement vectors used to define the ME surface will be null or have small magnitudes. In these cases, adaptations to the method need to be considered to avoid algebraic singularities or instable orientations, since small errors in the determination of the joints position can result in noisy orientations or even in the inversion of the local reference frame. A possible strategy to avoid this problem would be to use the normal vector computed in the previous time frame to define the segment orientation.

ME method can also be sensitive to the acquisition frequency of the system in use. For high frequencies, the displacement vector between time frames can present a small magnitude and, as in the previous case, if the data has noise, instabilities can occur during the calculation of segment orientation.

Regarding sample size, although experimental data was collected from six subjects, we consider that the number of gait cycles analyzed was sufficient to evaluate the ability of ME to estimate the longitudinal rotations of arms, forearms, thighs, and legs during normal gait with only 2 points per segment.

Despite these limitations, for movements characterized by smooth translations and rotations, the ME method performs well, providing a strong correlation with the orientations computed using the more complex biomechanical model. Moreover, the proposed method is not restrained to movements in sagittal plane: the main requirements to apply ME are for the movement to be non-stationary (e.g., not standing in the same position or adopting the same pose), to be smooth and continuous throughout time, and easily trackable with a minimal set of markers. Hence, ME can be applied to any movement in any anatomic

plane, as long as it is not composed by static motions or pure axial rotations.

In conclusion, this work presents an efficient method to estimate the orientation of body segments in stick figure models. Based on the surface generated by tracing the evolution of the segment in space, the ME method defines an orthogonal vector that depicts its rotation over time. This feature allows for the estimation of a plausible orientation for the segment, complementing the kinematic data with intrinsic information existent in the movement patterns. Due to the versatility and computational efficiency of the method, it can be easily applied in real-time applications to support the kinematic data retrieved from the common optical markerless systems, extending its use in clinical and rehabilitation environments. When applied to gait, this method produced good results for most body segments. Hence, the proposed method seems to be a valid tool to estimate orientations of stick figure models in smooth movements when the kinematic information is scarce. As future work, we aim to test our approach with a larger segment of the population and a greater variety of movement types to further validate our ME method. For instance, we expect that our approach can easily scale beyond movements predominantly occurring in the sagittal plane (e.g., gait) and towards other movements in frontal or transverse planes. We also intend to explore the validity of the ME method in the study of pathological populations to assess if the method is sensible to identify kinematic differences and compensatory movements.

## Disclosure statement

No potential conflict of interest was reported by the authors.

## Ethics approval

Ethical approval for this study was obtained from ethics committee of Instituto Superior Técnico in January 2020 with reference number 1/2020 (CE-IST).

## Funding

This research was supported by the Fundação para a Ciência e a Tecnologia through grants with references UIDB/50022/2020, UIDB/50021/2020, UTAP-EXPL/CA/0065/2017, and PTDC/CCI-COM/30274/2017.

**ORCID**

Miguel Tavares da Silva  <http://orcid.org/0000-0001-7056-4555>  
 Daniel Simões Lopes  <http://orcid.org/0000-0003-0917-9396>

**References**

- Alves T, Carvalho H, Lopes DS. 2020. Winning compensations: Adaptable gaming approach for upper limb rehabilitation sessions based on compensatory movements. *J Biomed Inform.* 108:103501.
- Bezodis IN, Cowburn J, Brazil A, Richardson R, Wilson C, Exell TA, Irwin G. 2020. A biomechanical comparison of initial sprint acceleration performance and technique in an elite athlete with cerebral palsy and able-bodied sprinters. *Sports Biomech.* 19(2):189–200.
- Cai L, Ma Y, Xiong S, Zhang Y. 2019. Validity and reliability of upper limb functional assessment using the Microsoft Kinect V2 sensor. *Appl Bionics Biomech.* 2019:1–14.
- Cao Z, Simon T, Wei SE, Sheikh Y. 2017. Realtime multi-person 2D pose estimation using part affinity fields. In *Proceedings of the IEEE Conference on Computer Vision and Pattern Recognition.* p. 1302–1310.
- Chakraborty S, Nandy A, Yamaguchi T, Bonnet V, Venture G. 2020. Accuracy of image data stream of a markerless motion capture system in determining the local dynamic stability and joint kinematics of human gait. *J Biomech.* 104:109718.
- Çubukçu B, Yüzgeç U, Zileli R, Zileli A. 2020. Reliability and validity analyzes of Kinect V2 based measurement system for shoulder motions. *Med Eng Phys.* 76:20–31.
- Davis RB, Ounpuu S, Tyburski D, Gage JR. 1991. A gait analysis data collection and reduction technique. *Hum Mov Sci.* 10(5):575–587.
- Gammon M, Udhani R, Patekar P, Sakamoto Y, Menon C, Irani P. 2020. Limb-O: real-time comparison and visualization of lower limb motions. In *Proceedings of the 11th Augmented Human International Conference (AH '20)*. Association for Computing Machinery, New York, NY, USA, Article 5, 1–8. DOI:10.1145/3396339.3396360
- Geerse DJ, Coolen BH, Roerdink M. 2015. Kinematic validation of a multi-Kinect v2 instrumented 10-meter walkway for quantitative gait assessments. *PLoS One.* 10(10):e0139913–15.
- Genevois C, Reid M, Creveaux T, Rogowski I. 2020. Kinematic differences in upper limb joints between flat and topspin forehand drives in competitive male tennis players. *Sports Biomech.* 19(2):212–226.
- Guess TM, Razu S, Jahandar A, Skubic M, Huo Z. 2017. Comparison of 3D joint angles measured with the Kinect 2.0 skeletal tracker versus a marker-based motion capture system. *J Appl Biomech.* 33(2):176–181.
- Harari Y, Bechar A, Riemer R. 2020. Workers' biomechanical loads and kinematics during multiple-task manual material handling. *Appl Ergon.* 83:102985 (13 pages).
- Kobsar D, Osis ST, Jacob C, Ferber R. 2019. Validity of a novel method to measure vertical oscillation during running using a depth camera. *J Biomech.* 85:182–186.
- Lopes DS, Silva MT, Ambrósio JA. 2013. Tangent vectors to a 3D surface normal: a geometric tool to find orthogonal vectors based on the Householder transformation. *CAD Comput Aided Des.* 45(3):683–694.
- Lopes DS, Faria A, Barriga A, Caneira S, Baptista F, Matos C, Neves AF, Prates L, Pereira AM, Nicolau H. 2019. Visual biofeedback for upper limb compensatory movements: a preliminary study next to rehabilitation professionals. In *Eurographics 2019 - Posters Track.*
- Ludewig PM, Cook TM. 2000. Alterations in shoulder kinematics and associated muscle activity in people with symptoms of shoulder impingement. *Phys Ther.* 80(3):276–291.
- Ma Y, Mithraratne K, Wilson NC, Wang X, Ma Y, Zhang Y. 2019. The validity and reliability of a kinect v2-based gait analysis system for children with cerebral palsy. *Sensors (Switzerland).* 19(7):1660.
- Matias NV, Roura I, Gonçalves S, da Silva MT, Lopes DS. 2021. Estimating anatomically plausible segment orientations using a kinect one sensor. *Ann Med.* 53(sup1):S143–S144.
- McDonald AC, Mulla DM, Keir PJ. 2019. Muscular and kinematic adaptations to fatiguing repetitive upper extremity work. *Appl Ergon.* 75(February 2018):250–256.
- Mehta D, Sotnychenko O, Mueller F, Xu W, Elgharib M, Fua P, Seidel HP, Rhodin H, Pons-Moll G, Theobalt C. 2020. XNect: real-time multi-person 3D motion capture with a single RGB camera. *ACM Trans Graph.* 39(4):1–24.
- Mehta D, Sridhar S, Sotnychenko O, Rhodin H, Shafiei M, Seidel HP, Xu W, Casas D, Theobalt C. 2017. VNect: real-time 3D human pose estimation with a single RGB camera. *ACM Trans Graph.* 36(4):1–13.
- Quental C, Azevedo M, Ambrósio J, Gonçalves SB, Folgado J. 2018. Influence of the musculotendon dynamics on the muscle force-sharing problem of the shoulder—a fully inverse dynamics approach. *J Biomech Eng.* 140(7):071005 (11 pages).
- Safaeepour Z, Esteki A, Ghomshe F, Abu Osman N. 2014. Quantitative analysis of human ankle characteristics at different gait phases and speeds for utilizing in ankle-foot prosthetic design. *Biomed Eng Online.* 13(1):19.
- Schneider PJ, Eberly DH. 2003. *Geometric tools for computer graphics.* 1st ed. Morgan Kaufmann.
- Shotton J, Sharp T, Fitzgibbon A, Blake A, Cook M, Kipman A, Finocchio M, Moore R. 2013. Real-Time human pose recognition in parts from single depth images. *Commun ACM.* 56(1):116–124.
- Sutherland DH. 2002. The evolution of clinical gait analysis: part II kinematics. *Gait Posture.* 16(2):159–179.
- Taylor JB, Westbrook AE, Head PL, Glover KM, Paquette MR, Ford KR. 2020. The single-leg vertical hop provides unique asymmetry information in individuals after anterior cruciate ligament reconstruction. *Clin Biomech (Bristol, Avon).* 80:105107.
- van Rossum G, Drake Jr FL. 2006. *Python/C API Manual - Python 2.6: (Python Documentation Manual Part 4).* Createspace Independent Publishing Platform Scotts Valley, California, US.
- Worthen-Chaudhari LC, McNally MP, Deshpande A, Bakaraju V. 2020. In-home neurogaming: demonstrating

- the impact of valid gesture recognition method on high volume kinematic outcomes. *J Biomech.* 104:109726.
- Wu G, Siegler S, Allard P, Kirtley C, Leardini A, Rosenbaum D, Whittle M, D'Lima DD, Cristofolini L, Witte H, et al. 2002. ISB recommendation on definitions of joint coordinate system of various joints for the reporting of human joint motion — Part I: ankle, hip, and spine. *J Biomech.* 35(4):543–548.
- Wu G, van der Helm FCT, Veeger HEJD, Makhsous M, Van Roy P, Anglin C, Nagels J, Karduna AR, McQuade K, Wang X, et al. 2005. ISB recommendation on definitions of joint coordinate systems of various joints for the reporting of human joint motion—Part II: shoulder, elbow, wrist and hand. *J Biomech.* 38(5):981–992.
- Zhang X, Dekel T, Xue T, Owens A, He Q, Wu J, Mueller S, Freeman WT. 2018. MosculP: Interactive visualization of shape and time. In: *Proceedings of the 31st Annual ACM Symposium on User Interface Software and Technology*; p. 275–285.